Dalton Transactions

ROYAL SOCIETY OF CHEMISTRY

PAPER

View Article Online
View Journal | View Issue

Cite this: *Dalton Trans.*, 2024, **53**, 16956

Redox properties of [Cp*Rh] complexes supported by mono-substituted 2,2′-bipyridyl ligands†

Jonah P. Stiel,‡[a] Wade C. Henke,§[a] William N. G. Moore,‡[a] Nathaniel M. Barker,¶[b] Allen G. Oliver,[b] Victor W. Day[a] and James D. Blakemore*[a]

The redox properties of half-sandwich rhodium complexes supported by 2,2′-bipyridyl (bpy) ligands can be readily tuned by selection of an appropriately substituted derivative of bpy, but the influences of single substituents on the properties of such complexes are not well documented, as disubstituted bpy variants are much more common. Here, the synthesis, characterization, and redox properties of two new [Cp*Rh] complexes (where Cp* is η^5-1,2,3,4,5-pentamethylcyclopentadienyl) supported by the uncommon mono-substituted ligands 4-chloro-2,2′-bipyridyl (mcbpy) and 4-nitro-2,2′-bipyridyl (mnbpy) are reported. Single-crystal X-ray diffraction studies and related spectroscopic experiments confirm installation of the single substituents (−Cl and $-NO_2$, respectively) on the bipyridyl ligands; the precursor mono-substituted ligands were prepared *via* a divergent route from unsubstituted bpy. Electrochemical studies reveal that each of the complexes undergoes an initial net two-electron reduction at potentials more positive than that associated with the parent unsubstituted complex of bpy, and that the complex supported by mnbpy can undergo a third, chemically reversible reduction at –1.62 V *vs.* ferrocenium/ferrocene. This redox behavior is consistent with inductive influences from the substituent groups on the supporting ligands, although the nitro group uniquely enables addition of a third electron. Spectrochemical studies carried out with UV-visible detection confirm the redox stoichiometry accessible to these platforms, highlighting the rich redox chemistry and tunable behavior of [Cp*Rh] complexes supported by bpy-type ligands.

Received 6th August 2024,
Accepted 23rd September 2024

DOI: 10.1039/d4dt01766h

rsc.li/dalton

Introduction

Understanding and, ultimately, controlling the redox properties of well-defined metal complexes are key goals in the fields of redox chemistry and molecular electrocatalysis. Organometallic complexes in particular attract significant attention in these realms, due to their important roles as catalysts and redox mediators. Control over the redox properties of metal complexes can be exercised with a variety of strategies; these include modifying ligands with electron donating or electron withdrawing substituents that can drive inductive and resonance effects,[1] using "non-innocent" ligands that are redox-active[2–5] or proton-responsive,[6–9] developing multimetallic species,[10–14] and immobilizing complexes on electrode surfaces,[15–17] among others. However, determining the precise origin of modified redox chemistry within even closely related families of complexes often requires significant effort; small changes to ligands supporting organometallic complexes can result in significant changes in chemical and/or electrochemical properties.[18,19]

The 2,2′-bipyridyl (bpy) ligand platform is ubiquitous in inorganic and organometallic chemistry and is perhaps the most well-studied chelating ligand.[20] The high stability, ease of preparation, and demonstrated catalytic, photophysical, and redox properties of compounds supported by bpy have led to numerous successful investigations aimed at tuning the properties of complexes by modification of bpy.[19,21] In our own group, we have been especially interested in the installation of electron donating (ED) or electron withdrawing (EW) groups as a strategy for tuning of the redox properties of the parent metal complexes. Installation of ED or EW groups can alter the π-accepting ability of the conjugated bpy framework as well as

[a]*Department of Chemistry, University of Kansas, 1567 Irving Hill Road, Lawrence, Kansas 66045, USA. E-mail: blakemore@ku.edu*
[b]*Department of Chemistry & Biochemistry, University of Notre Dame, 149 Stepan Chemistry Hall, Notre Dame, Indiana 46545, USA*

†Electronic supplementary information (ESI) available: Spectroscopic (NMR, EAS), electrochemical, and crystallographic (XRD) data. CCDC 2203159, 2203160 and 2370048. For ESI and crystallographic data in CIF or other electronic format see DOI: https://doi.org/10.1039/d4dt01766h

‡Current address: Department of Chemistry, University of California at Irvine, Irvine, California 92617, USA.
§Current address: Procter & Gamble, North Chicago Plant, 3500 16th St, North Chicago, Illinois 60064, USA.
¶Current address: Integrated Molecular Structure Education and Research Center (IMSERC), Northwestern University, Evanston, Illinois 60208, USA.

the σ-donating ability of the imine nitrogens. We have found recently that modifying the ligand bite angle by substitution of bpy with 4,5-diazafluorene-type (daf-type) ligands can provide an alternative means of tuning electronic properties while retaining the diimine-type donor configuration offered by the more common bpy.[22,23] This strategy relies on subtle diminishment of the degree of metal–ligand orbital overlap to achieve redox tuning, and we have found it to be effective in affording a measure of control over reduction potentials.[24,25]

Other bidentate ligands can also be used in place of bpy in studies of redox chemistry and catalysis. In our own group, bidentate bisphosphine ligands have been especially useful for comparison to bpy.[26–28] We have found that [Cp*Rh] complexes are able to form quite stable half-sandwich metal hydrides upon protonation of appropriately reduced precursors that can be supported by the diphosphines. These isolable hydrides[29] are notable for their structural similarity to the transient, reactive hydrides formed by more common bpy-supported analogues.[30–34] In principle, enhanced back-bonding from the metal center to the phosphorus donor atoms can be envisioned to result in diminished hydricity in the bisphosphine-supported systems and thus lowered reactivity.[35] Characterization of the bisphosphine analogues has served as a useful strategy for elucidation of such electronic influences over hydride generation, a process of relevance to catalytic H_2 evolution and also other hydride-transfer reactions which can be carried out by [Cp*Rh] species.[36–38]

In the course of our investigations on the redox properties of [Cp*Rh] complexes, we were surprised to find that little work has examined how the chemical or electrochemical properties of rhodium complexes can be modulated by singly-substituted, non-C_{2v}-symmetric 2,2′-bipyridyl ligands. Hartl and co-workers did report the synthesis and a thorough exploration of the redox properties of a chloro-substituted terpyridine complex of rhodium (**H**, see Chart 1) in 2004. On the other hand, we are unaware of any studies of the redox chemistry of [Cp*Rh] complexes supported by mono-substituted bpy ligands, although we have been interested in such species for some time.[39]

In prior work, we have also explored the redox tuning accessible with 4,4′-bis-(*tert*-butyl)-2,2′-bipyridyl,[19] 4,4′-bis(trifluoromethyl)-2,2′-bipyridyl,[19] and perhaps most uniquely, 4,4′-dinitro-2,2′-bipyridyl (dnbpy).[1] Use of dnbpy affords a [Cp*Rh] complex (**M**) with markedly unique reductive electrochemical properties; **M** first undergoes a ligand-centered reduction before undergoing three further metal- and/or ligand-centered reductions, contrasting with the net $2e^-$ ECE-type behavior displayed by most other [Cp*Rh] complexes that have been studied. We anticipated that pursuing the preparation and study of [Cp*Rh] complexes supported by mono-substituted bpy ligands could shed new light on the influence of substituents on the resulting redox chemistry, particularly in the case of the nitro group.

Here, we report the synthesis, characterization, and redox properties of two half-sandwich rhodium complexes supported by non-C_2-symmetrical, mono-substituted 2,2′-bipyridyl ligands bearing either chloro (–Cl, as in **1**) or nitro (–NO_2, as in **2**) substituents. We find that **1** and **2** display electrochemical profiles that are intermediate between the analogous complexes supported by bpy (**B**) and dnbpy (**M**). Single-site nitration in 4-nitro-2,2′-bipyridyl (mnbpy) enables an additional $1e^-$ reduction for **2** that is not accessible to **1** or **B**, suggesting a unique role in this redox chemistry. Structural data from single-crystal X-ray diffraction analysis for **1** and **2** show that the lowered symmetry of the bpy-type ligand platform results in only minor perturbations to the structural properties of the [Cp*Rh] cores of the complexes, while electrochemical data collected in acetonitrile (MeCN) electrolyte reveal a significant shift in reduction potentials induced by incorporation of the nitro substituent in **2**. Taken together with spectrochemical redox titration data, these results provide insight into the properties of the reduced forms of both **1** and **2**. Our results show that the use of mono-substituted bpy-type ligands represents an attractive strategy for tuning the redox properties of [Cp*Rh] complexes.

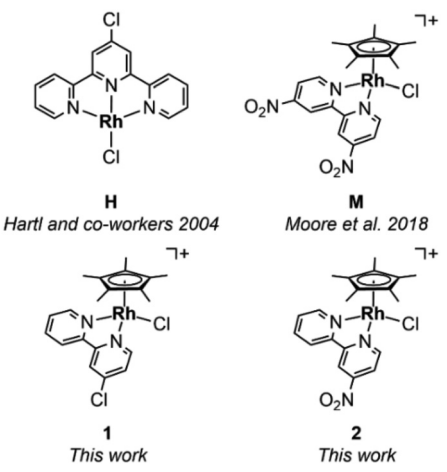

Chart 1 Rhodium complexes of relevance to the work reported here.

Results and discussion

In order to access **1** and **2**, we used a divergent synthetic route assembled from four established procedures from the literature that have not before been combined in sequence for the preparation of mcbpy and mnbpy.[40–42] Our strategy centers on preparation of mono-nitrobipyridine-*N*-oxide (mnbpy-*N*-oxide) as a key synthon from which both of the desired ligands could be readily prepared. The synthesis begins with oxidation of readily available 2,2′-bipyridine to form 2,2′-bipyridine-1-oxide (bpy-*N*-oxide) (see Scheme 1) according to the procedure of Aukaloo and co-workers.[40] The mono-*N*-oxide product, being lower symmetry than the parent bpy, can engage in further non-symmetric reactivity useful for our purpose here; selective nitration of bpy-*N*-oxide at the 4-position generates mononitrobipyridine-*N*-oxide (mnbpy-*N*-oxide). The nitration was

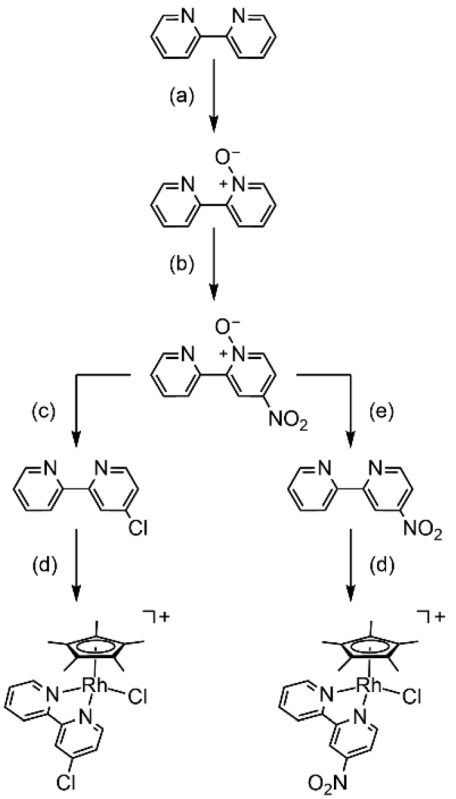

Scheme 1 Divergent synthesis of **1** and **2** from 2,2′-bipyridyl. (a) Trifluoroacetic acid, 30% H_2O_2; 25 °C. As described in ref. 40. (b) Red fuming nitric acid, conc. H_2SO_4; 100 °C. As described in ref. 40. (c) **1**. Acetic acid, acetyl chloride; 100 °C. 2. PCl_3; 65 °C. As described in ref. 41. (d) $[Cp^*RhCl_2]_2$, $AgPF_6$ in CH_2Cl_2 with limited MeCN as solvent; 25 °C. (e) PCl_3; 65 °C. As described in ref. 42.

also carried out according to a procedure from Aukaloo and co-workers.[40] Sequential reaction of this product with acetyl chloride in glacial acetic acid and excess phosphorous(III) chloride provides the desired mcbpy; these reactions were carried out according to Mizuno *et al.*[41] And finally, we followed the procedure of Mann and co-workers to prepare mnbpy by reaction of mnbpy-*N*-oxide with PCl_3.[42]

The dimeric $[Cp^*RhCl_2]_2$ complex developed by Maitlis and co-workers[43,44] was found to be useful for the preparation of **1** and **2**, building on the reliable propensity of this material to form half-sandwich complexes when exposed to suitable bidentate chelating ligands.[45,46] Reaction of 0.5 equiv. of $[Cp^*RhCl_2]_2$ with 1.05 equiv. of $AgPF_6$ followed by removal of the AgCl precipitate and addition of 1.05 equiv. of mcbpy or mnbpy gave good yields (>85%) of **1** and **2**, respectively, as orange-yellow, air-stable solids. No unusual behaviors were encountered in these syntheses, although use of a two-part solvent system (CH_2Cl_2 containing 30 drops of MeCN; see Experimental section) was required, ostensibly to promote binding of the bidentate ligands to the [Cp*Rh] core. This behavior resembles that which we encountered in work with dnbpy, in that more weakly coordinating tetrahydrofuran was required for successful coordination of the relatively electron-deficient dnbpy to the [Cp*Rh] core in that case.[1]

The products of the syntheses were characterized by ^1H, $^{13}C\{^1H\}$, ^{19}F, and ^{31}P NMR spectroscopy, confirming generation of the desired complexes in both cases (see ESI, Fig. S1–S8†). The ^1H-NMR spectrum of **1** contains six unique aromatic resonances, in accord with the expected C_1 symmetry of the complex and a coincidental overlap of two of the seven expected signals; the ^1H NMR spectrum of **2** contains all seven expected aromatic resonances. Both spectra also contain the expected singlets integrating to 15 protons in the alkyl region, confirming the presence of the five equivalent methyl groups of the freely-rotating Cp* moiety. The $^{13}C\{^1H\}$ NMR spectra of **1** and **2** reveal resonances associated with the Cp* ring carbons; these are split by the 100% abundant $I = 1/2$ ^{103}Rh metal centers ($^1J_{C,Rh}$ values are 8.2 and 9.2 Hz, respectively, for **1** and **2**). ^{19}F and ^{31}P NMR spectra for **1** and **2** are very similar, confirming the presence of the outer-sphere hexafluorophosphate counter-anions.

Single crystals of **1** and **2** suitable for X-ray diffraction analysis were grown by vapor diffusion methods in both cases (see Experimental section). The resulting structures (see Fig. 1)

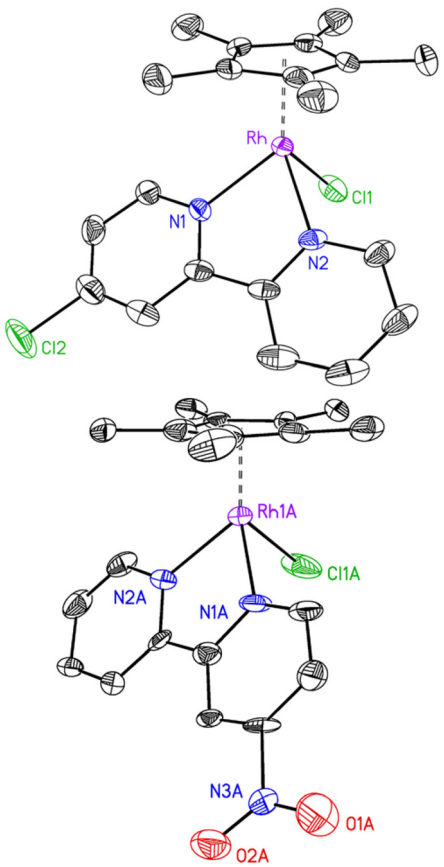

Fig. 1 Solid-state structures of the [Cp*Rh] complexes reported in this work. Upper structure: major enantiomer of **1** that is present 85% of the time in the asymmetric unit (structure q01i). Lower structure: first of two ordered enantiomers of **2** present in the asymmetric unit in space group $Pna2_1$ (structure: a11a-No33). Displacement ellipsoids are shown at the 50% probability level. Hydrogen atoms, outer-sphere counter-anions, and minor components of apparent disorder for **1** are omitted for clarity.

Table 1 Selected bond lengths and distances for the [Cp*Rh] complexes discussed here

	Bond lengths[a] [Å]				Bond angles[a] [°]		
Compound	Rh–N	Rh–Cp*$_{cent}$	Rh–Cl	d_{C-C} [b]	∠N–Rh–N	θ (∠Cp*$_{cent}$–Rh–N1/N2$_{cent}$)[c]	Ref.
1 [d]	2.106(4)	1.790	2.401(1)	1.469(7)	76.3(2)	144.4	This work
2 [e]	2.112(12)	1.778	2.377(4)	1.46(2)	76.7(4)	147.8	This work
B	2.140(7)	1.774	2.379(3)	1.49(2)	75.3(4)	147.7	47
M	2.114(2)	1.787	2.400(1)	1.473(3)	76.4(1)	145.6	1
A	2.099(4)	1.784	2.423(1)	1.472(7)	76.7(2)	144.3	48

[a] Values are given as the arithmetic mean of the values of the parameters for independent molecular species in the structural data. Stated e.s.d.'s on distances were taken as the largest among the individual values for the independent molecular species in the refined structural data. [b] Defined as the distance between the two central carbons interconnecting the two pyridyl rings. [c] Refers to the angle between the Cp* ring centroid, the Rh center, and the midpoint of the N1···N2 vector within the diimine ligand. [d] Values correspond to structure code q01i; see ESI, Fig. S24 and S25.† [e] Values correspond to the average of two crystallographically-independent molecules present in asymmetric unit for structure code a11a-No33, see ESI Fig. S26 and S27.†

confirm that the first coordination spheres of the synthesized complexes contain the [η^5-Cp*] ligand, the expected κ^2-diimine ligand, and a single chloride ligand bound to the [Cp*Rh] core. The bond metrics (see Table 1) for **1** and **2** show that, generally speaking, the rhodium centers are not strongly affected by the single substituents in the new complexes. For example, the similarities of the Rh–Cl and Rh–Cp*$_{cent}$ distances are consistent with the formal oxidation state (+III) for both of the rhodium centers. Bond distances and angles for **1** and **2** are also comparable to those in the parent [Cp*Rh(bpy)Cl]$^+$ (**B**),[47] to those in **M** supported by dnbpy,[1] and to those in an analogous [Cp*Rh] complex supported by the 4-amino-2,2′-bipyridyl ligand (**A**) that we have previously reported.[48,49] On the basis of these comparisons, we conclude that inclusion of a single substituent on bpy does not markedly perturb the structural properties of the [Cp*Rh] core.

Of note, our structure of **2** is the only one available for a metal complex supported by mnbpy, as judged by a search of the Cambridge structural database (CSD).[50] There are, however, two structures of the mono-*N*-oxide of mnbpy.[51] Additionally, a search of the CSD revealed that there are only two structures featuring mcbpy, although these correspond to large, multinuclear complexes.[52] The paucity of structures of mononuclear metal complexes of mcbpy and mnbpy may be attributable to the non-routine nature of the solid-state structures associated with their complexes, as judged by the details associated with those of **1** and **2** (see ESI, pp. S21–S28† for details).

In our structure, as in those of metal complexes supported by dnbpy, the –NO_2 group is approximately co-planar with the partnered pyridine ring; the dihedral angles between the mean planes of the [C_5N] pyridine rings and the planar C···NO_2 groupings in crystallographically-independent molecules A and B of **2**, are 6.6° and 8.3°, respectively. The observed but sterically unfavorable near co-planarity of the –NO_2 groups and the pyridine rings of the bpy core in both crystallographically-independent molecular cations of **2** found in the structure (see ESI, pp. S24 and S25† for details) suggested to us that there could be a strong electronic influence of the substituent on both the π-system of the ligand and, in turn, the metal core of the complex; the electrochemical data (*vide infra*) confirmed this to be the case.

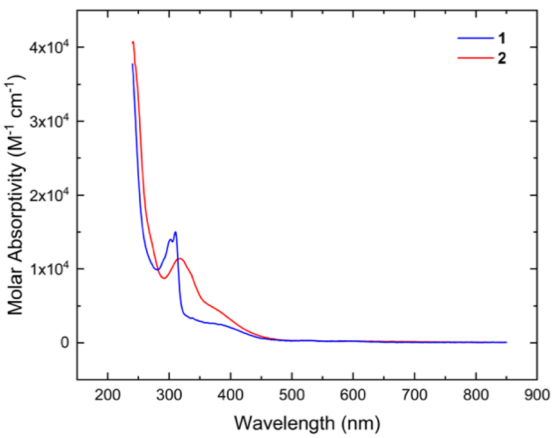

Fig. 2 Electronic absorption spectrum of **1** and **2** at concentrations of 62 μM and 63 μM, respectively.

Further characterization of **1** and **2** was performed with electronic absorption (EA) spectroscopy. The spectrum of **1** displays a relatively sharp bifurcated absorption at 310 nm with a molar absorptivity greater than 10 000 M^{-1} cm^{-1} (see Fig. 2). The shape of this absorption is typical of analogous complexes supported by unsubstituted bpy.[1] In contrast, the EA spectrum of **2** does not display this bifurcated fingerprint, and there is a broader absorption feature with λ_{max} at 318 nm. This loss of the distinctive bifurcation is also seen with **M**, suggesting that this behavior is characteristic of nitro-substituted derivatives of **B** and attributable to the unique electronic structures engendered by the nitro-substituted ligands.[53]

To interrogate the electrochemical properties of the new complexes, cyclic voltammetry was performed inside an inert atmosphere glovebox. The CV data for **1** reveal a dominant, quasi-reversible reduction event centered at −1.19 V *vs.* ferrocenium/ferrocene (denoted hereafter as $Fc^{+/0}$; see Fig. 3, blue data). By comparison, **B** displays a single, 2e$^-$ reduction event centered at (−1.21 V *vs.* $Fc^{+/0}$).[54] In the case of **B**, the redox

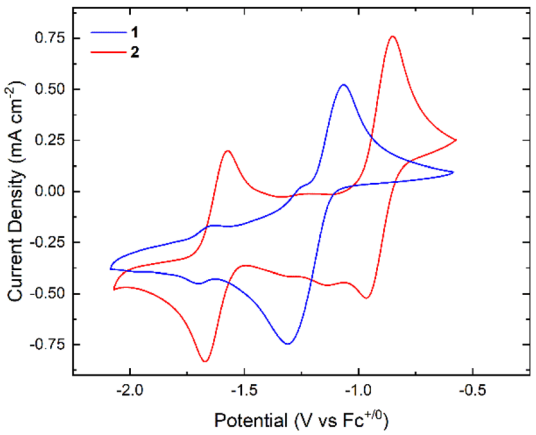

Fig. 3 Cyclic voltammograms of **1** and **2**. **1** has a single, 2e$^-$ redox couple that is reminiscent of that of the parent bpy complex. **2** has a 2e$^-$ redox couple followed by a further, more uncommon 1e$^-$ redox couple.

couple has been assigned as associated with formal rhodium(III)/rhodium(I) redox cycling; in this event, reduction is associated with loss of the inner-sphere chloride ligand.[55–57] In our own work, we have measured a peak-to-peak separation (ΔE_p) of *ca.* 250 mV for reduction of **B**,[19] confirming the significant chemical changes associated with the multistep processes involved in reduction of rhodium(III) to rhodium(I).[4] In accord with these prior findings, **1** displays a ΔE_p of *ca.* 245 mV, and thus its redox behavior is virtually identical in appearance to that exhibited by **B**. Therefore, it was also assigned as a net 2e$^-$ reduction associated with conversion of rhodium(III) to rhodium(I) with loss of chloride. Consistent with this assignment, the $E_{1/2}$ value for **1** is shifted positive relative to that of **B** by 20 mV; this confirms that the chloro substituent exhibits a minor influence on the redox cycling of the system. In the cases of both **B** and **1**, the significant deviation of the ΔE_p value from that expected for a fully electrochemically reversible process (28.5 mV) can be attributed to the chemical/structural changes in the complex upon reduction. The 2e$^-$ reduced form of **B** is a T-shaped complex[57] with significant delocalization of electron density into the bipyridyl π-system; it is sensible, given the similar voltammetric profile, that the 2e$^-$ reduced form of **1** is also a T-shaped species. We also note that under our selected experimental conditions the ferrocenium/ferrocene couple typically displays a ΔE_p value of *ca.* 70, not much larger than the ideal value for a 1e$^-$ electrochemically reversible couple of 57 mV.

However, in addition to this primary redox event observed for **1**, a minor electrochemically quasi-reversible couple was also observed at *ca.* −1.7 V *vs.* Fc$^{+/0}$. On the basis of this reduction potential and the quasi-reversible appearance of the wave, we have assigned this couple as redox cycling of electrogenerated $[Cp^*RhCl]_2$,[58,59] a reduced form of Maitlis' useful $[Cp^*RhCl_2]_2$. We have previously observed redox cycling associated with electrogenerated $[Cp^*RhCl]_2$ at potentials near −1.8 V.[60] Here, we also anticipate that this minor impurity is electrogenerated upon reduction of **1**; loss of bidentate ligands from the [Cp*Rh] core upon reduction appears to be promoted by the lability incurred by the rhodium(II) oxidation state.[60] Considering all this, **1** is quite similar to **B**, but with an apparent lower degree of stability upon reduction; the observation of formation and redox cycling of $[Cp^*RhCl]_2$ suggests that mcbpy could be more readily lost from the rhodium center than bpy, perhaps in line with its less electron-donating nature and/or lower symmetry. At this stage, we anticipate that the slight shift in the reduction potential associated with $[Cp^*RhCl]_2$ between our prior work given in ref. 60 and in the present study is attributable to poor chemical reversibility and/or differences in the concentrations of this species present at the electrode across the two different systems under investigation.

The cyclic voltammogram of **2** is significantly more complex than those of **1** and **B**. Two primary redox couples could be observed in our experiments: a large couple centered at −0.91 V and a smaller couple centered at −1.62 V. On the basis of the current passed, it appears that the first wave is *ca.* 2× the height of the first; we thus assign the first reduction as a net 2e$^-$ couple and the second as a 1e$^-$ couple. This proposal is supported by spectrochemical titration data (*vide infra*). The ΔE_p values of the two waves are *ca.* 120 mV and 100 mV, respectively, placing them in the electrochemically quasi-reversible realm, but both waves do appear largely chemically reversible on the basis of the near-unity ratios of their background-corrected peak cathodic and anodic currents ($i_{p,a}/i_{p,c}$ values). Within our assignment, the first couple is associated with reduction from rhodium(III) to rhodium(I), although this process is shifted positively by 300 mV in comparison to the value of $E_{1/2}$ measured for **B**. This can be attributed to the strongly electron withdrawing nature of the nitro functional group.

The second chemically reversible reduction at −1.62 V is more challenging to assign. However, our prior work with the 4,4′-dinitro-2,2′-bipyridyl derivative, **M**, can provide some insight.[1] **M** undergoes four 1e$^-$ reductions in its cyclic voltammetric response; in our work, these could be assigned to two dnbpy-centered reductions and two rhodium-centered reductions (starting with Rh(III) and proceeding to Rh(II) and Rh(I)). Among these reductions of **M**, the most positive was associated with dnbpy itself; EPR data suggest the first reduction of **M** is ligand centered.[1] On this basis, we propose that the reduction of **2** observed at $E_{1/2}$ = −1.62 V is associated with dnbpy-centered reduction; this proposal is summarized graphically in Fig. 4 below. Importantly we note here that redox associated with $[Cp^*RhCl]_2$ can be excluded as contributing to the observed wave at −1.62 V, as the redox associated with this compound is not highly reversible,[60] as in the response obtained here for **2**.

Within this model, we note that the family of complexes formed by **B**, **2**, and **M** represents a homologous series in which the number of nitro groups varies from 0 to 1 to 2. Notably, the addition of each nitro group to the bpy core enables an additional 1e$^-$ ligand-centered reduction that is not observed in related non-nitrated derivatives (*i.e.*, dnbpy

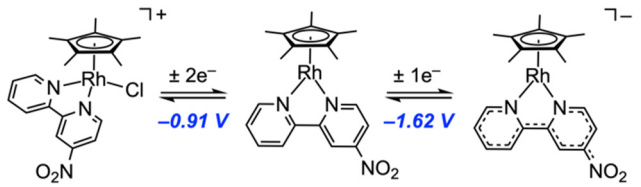

Fig. 4 Proposed assignment of the individual species formed upon reduction of compound **2** in the sequence of two observable redox events studied here. The first reduction is $2e^-$ in nature and occurs at −0.91 V and the second is $1e^-$ in nature and occurs at −1.62 V. The dashed bonds in the structure of the triply reduced species are intended to indicate reduction of the mnbpy ligand; the ligand-centered electron density in this species could be hosted by the 2,2′-bipyridyl core and/or the nitro group.

can be directly reduced twice whereas mnbpy can be reduced once). This latter point is confirmed by the properties of **1**; although **1** features the electron-withdrawing chloro substituent, it displays redox properties most closely aligned with those of **B**, as it lacks any nitro groups. At the far end of our homologous series of nitrated complexes, the very electron-poor dnbpy ligand also "splits" the normally multielectron reduction of [Cp*Rh] complexes into two distinct $1e^-$ events; double nitration shifts the ligand-centered reduction significantly positive, such that the dnbpy core is reduced at a potential more positive than those associated with the formal rhodium-centered reductions. For **2**, however, the situation is also intermediate in this respect, as formal rhodium-centered reduction precedes the direct mnbpy reduction.

In order to spectroscopically probe the properties of the reduced forms of **1** and **2**, we next carried out spectrochemical titrations with UV-visible monitoring. This procedure was performed by titrating a solution of **1** or **2** in MeCN with increasing equivalents of decamethylcobaltocene (Cp^*_2Co) while monitoring spectral changes with UV-visible absorption spectroscopy. Cp^*_2Co was selected as the chemical reductant for this purpose as its reduction potential ($E_{1/2}$ = −1.91 V *vs.* $Fc^{+/0}$ in MeCN[61]) is significantly more negative than those associated with the reductions measured for **1** and **2**.

Treatment of **1** with increasing equivalents of Cp^*_2Co (up to 2 eq.) resulted in new absorbances that grew in intensity at 298 nm, 525 nm, and 775 nm (see ESI, Fig. S20†). These features continue to grow with additions up to 2 equiv., confirming the $2e^-$ nature of the reduction of **1** inferred from the electrochemical data (*vide supra*). Furthermore, these features closely resemble those associated with Cp*Rh(bpy),[19,56] an observation consistent with the overall similarity of bpy and mcbpy. Isosbestic points at 230 nm and 247 nm were measured, indicating clean conversion of **1** into its formally rhodium(I) form. Importantly, the spectrum ceases evolving isosbestically when titrating beyond two equivalents of reductant, in accord with the assignment of net $2e^-$ electrochemistry. In light of all these results, the spectrochemical data suggest that one-electron reduction of **1** forms a transient species which undergoes disproportionation to form the doubly reduced rhodium(I) complex even upon addition of substoichiometric quantities of Cp^*_2Co. This tendency for [Cp*Rh] complexes to undergo reductive disproportionation is well documented, but can be overcome through use of specialized ligands that support disambiguation of the Rh^{III}/Rh^{II} and Rh^{II}/Rh^{I} reduction potentials.[4,60]

Reduction of **2** with Cp^*_2Co in a similar fashion also resulted in spectral changes that support our assignment of the redox properties implied by the electrochemical data (see ESI, Fig. S21†). To deconvolute the interpretation of the two distinct phases of spectral changes, data collected with **2** and up to two equivalents of the reductant were analyzed independently from the data collected with additions of two or more equivalents of Cp^*_2Co. Using this strategy, it was possible to identify the spectral changes occurring during the initial $2e^-$ reduction and those occurring during the separate $1e^-$ reduction. During the addition of the first two equivalents of reductant, new absorbances appeared at 297 nm, 370 nm, 460 nm, 685 nm, and 800 nm (see ESI, Fig. S22†). Isosbestic points at 232 nm, 256 nm, and 344 nm were also identified, indicating relatively clean conversion of the chemical species in the titration, despite the appearance of additional minor features in the electrochemical data. As in the case of **1**, observation of uniform spectral changes up to addition of 2 equiv. of Cp^*_2Co are consistent with the transient nature of the Rh(II) form of this compound and the overall reductive disproportionation pathway at work.

Further additions of another 1 eq. of Cp^*_2Co to the solution of **2** (up to three total equivalents of Cp^*_2Co per [Rh]) led to the growth of new peaks at 520 nm, 685 nm, and 800 nm (see ESI, Fig. S23†). The presence of a new set of isosbestic points at 235 nm and 253 nm indicates that the triply reduced **2** species can be generated and is stable on the timescale on which this titration was executed (1–2 h). This observation is also consistent with the chemically reversible nature of the related reduction wave measured by CV. As the addition of Cp^*_2Co beyond three equivalents led to no further isosbestic spectral changes, we conclude that these results confirm the assignment of the couple centered at −0.91 V *vs.* $Fc^{+/0}$ as being a $2e^-$ redox event and the couple centered at −1.62 V *vs.* $Fc^{+/0}$ as belonging to a $1e^-$ redox event.

The spectral changes associated with the third reduction of **2** primarily impact the long-wavelength features between 600 and 900 nm that can be concluded on the basis of prior work to be associated with intra-bpy transitions.[62] This provides support for our assignment of this reduction as mnbpy-centered, since such a reduction, particularly one centered in the π-system containing the nitro group itself,[53] could drive changes in the π-orbital energies within the bpy framework. Additionally, we note that these longer wavelength features are more intense for **2** than for **1**, a situation consistent with the greater electron withdrawing nature of the nitro substituent in **2** than the chloro in **1** (*cf.* $\varepsilon_{760} \approx 1700\ M^{-1}\ cm^{-1}$ for **1** *vs.* $\varepsilon_{800} \approx 4300\ M^{-1}\ cm^{-1}$ for **2**). This finding underscores the tunable nature of bpy ligands and the power of comparisons between derivatives to extract useful trends in spectroscopic data.

Considering all of these findings, we note that the solid-state data from XRD did not provide an indication of the significant difference in electrochemical properties of **1** and **2**. Indeed, it should be noted that compounds with quite similar structural parameters can have quite different redox properties, as has been found in a significant body of prior work. This is particularly appropriate in this case where inductive effects from peripheral substitution of ligand groups do not exert a dramatic *structural* influence over bonding around the metal–ligand core of the complexes under investigation but can result in significant *electronic* differences. Additionally, we note our ongoing enthusiasm for the approach of utilizing parallel chemical and electrochemical work to probe the redox properties and oxidation-state-dependent reactivity of metal complexes. By considering chemical and electrochemical data in a common frame of reference, a coherent understanding can often be obtained.

Conclusions

Here, we have reported the synthesis, characterization, and electrochemical properties of the [Cp*Rh] complexes **1** and **2** supported by mcbpy and mnbpy, respectively. The new complexes were found to be quite structurally similar to related derivatives supported by bpy, dnbpy, and mabpy in the solid state, but despite this, the use of the mono-substituted ligands dramatically alters the redox properties of the complexes. The redox behavior of **2** is intermediate between that of **B** and **M**, illustrating the utility of non-symmetric mono-substitution in enabling 'fine-tuning' of the redox properties of the complexes. The ability of **2** to undergo reduction by $3e^-$ underscores that nitro substituents are uniquely well suited for unlocking new reductive electrochemistry in organometallic complexes. Taken together, these results also underscore the great variety of electrochemical properties accessible to [Cp*Rh] complexes when prepared with suitable supporting ligands.

Experimental section

General considerations

All manipulations were carried out in dry N_2-filled gloveboxes (Vacuum Atmospheres Co., Hawthorne, CA, USA) or under an N_2 atmosphere using standard Schlenk techniques unless otherwise noted. All solvents were of commercial grade and dried over activated alumina using a PPT Glass Contour (Nashua, NH, USA) solvent purification system prior to use, and were stored over molecular sieves. All chemicals were obtained from major commercial suppliers. Deuterated solvents for NMR studies were purchased from Cambridge Isotope Laboratories (Tewksbury, MA, USA); CD_3CN was dried and stored over 3 Å molecular sieves.

^1H, $^{13}C\{^1H\}$, ^{19}F, and ^{31}P NMR spectra were collected on 400 or 500 MHz Bruker spectrometers (Bruker, Billerica, MA, USA). ^1H NMR spectra were referenced to the residual protio-solvent signal. Heteronuclear NMR spectra were referenced to the appropriate external standard following the recommended scale based on ratios of absolute frequencies (Ξ). ^{19}F NMR spectra are reported relative to CCl_3F and ^{31}P NMR spectra are reported relative to H_3PO_4.[63,64] Electronic absorption spectra were collected with an Ocean Optics Flame spectrometer equipped with a DH-Mini light source (Ocean Optics, Largo, FL, USA) using a quartz cuvette. Experimental high resolution mass spectrometry data were collected on a LCT Premier mass spectrometer equipped with a quadrupole, time-of-flight mass analyzer, and an electrospray ion source. Predicted mass spectrometry data were obtained from PerkinElmer Informatics' ChemDraw Professional Suite. Elemental analyses were performed by Midwest Microlab, Inc. (Indianapolis, IN, USA).

X-ray diffraction

Crystals were mounted on polyimide MiTeGen loops and placed under a cold nitrogen stream for data collection. For **1** (**q01i**), low temperature (200 K) X-ray data were collected using ω- or φ-scans on a Bruker Proteum diffractometer equipped with two CCD detectors (APEX II and Platinum 135) sharing a common MicroStar Microfocus Cu rotating anode generator (Cu Kα = 1.54178 Å) with Helios high-brilliance multilayer mirror optics. For **2** (**a11a**), low temperature (100 K) X-ray data were collected using ω- or φ-scans on a Bruker AXS D8 KAPPA diffractometer with an APEX II CCD detector and TRIUMPH graphite monochromator with Mo radiation (Mo Kα = 0.71073 Å). Preliminary lattice constants were obtained with SMART in the Bruker APEX2 (**q01i**) or APEX4 (**a11a**) Software Suite, while integrated reflection intensities for all compounds were produced using SAINT.[65,66] The data sets for **1** and **2** were corrected empirically for variable absorption effects with SADABS using equivalent reflections.[67,68] SHELXT was used to solve each structure using intrinsic phasing methods.[69] Final stages of weighted full-matrix least-squares refinement were conducted using F_o^2 data with SHELXL[70,71] in the Olex2 software package[72] or in SHELXle.[73] All non-hydrogen atoms were refined anisotropically. All hydrogen atoms were included into the model at geometrically calculated positions and refined using a riding model. The isotropic displacement parameters of all hydrogen atoms were fixed to 1.5 (methyl) or 1.2 (non-methyl) times the equivalent isotropic U value of the carbon atoms to which they are bonded. The relevant crystallographic and structure refinement data for the structures of **1** and **2** are given in Table S1.†

Electrochemistry

Electrochemical experiments were carried out in a nitrogen-filled glove box. 0.10 M tetra(n-butylammonium) hexafluorophosphate (SigmaAldrich; electrochemical grade) in acetonitrile served as the supporting electrolyte. Measurements were made with a Gamry Reference 600 Plus Potentiostat/Galvanostat using a standard three-electrode configuration. The working electrode was the basal plane of highly oriented pyrolytic graphite (HOPG, GraphiteStore.com, Buffalo Grove, Ill.; surface area: 0.09 cm^2), the counter electrode was a

platinum wire (Kurt J. Lesker, Jefferson Hills, PA; 99.99%, 0.5 mm diameter), and a silver wire immersed in electrolyte served as a pseudo-reference electrode (CH Instruments). The reference was separated from the working solution by a Vycor frit (Bioanalytical Systems, Inc.). Ferrocene (Sigma Aldrich; twice-sublimed) was added to the electrolyte solution at the conclusion of each experiment (~1 mM); the midpoint potential of the ferrocenium/ferrocene couple (denoted as $Fc^{+/0}$) served as an external standard for comparison of the recorded potentials. Concentrations of analyte for cyclic voltammetry were typically 1 mM.

Spectrochemical titrations

Spectrochemical titration experiments were carried out in a nitrogen-filled glove box. A 1 mM solution of decamethylcobaltocene (Cp^*_2Co) in acetonitrile was titrated into a cuvette filled with ~3 mL of a ~70 μM solution of **1** or **2** in acetonitrile. Data were collected with the Ocean Optics Flame spectrometer equipped with a DH-Mini light source. Titrant was added using a Hamilton syringe. The solution inside the cuvette was stirred with a magnetic stir bar to ensure homogeneity.

Synthetic procedures

Synthesis of [Cp*Rh(mcbpy)Cl]PF_6. To a suspension of $[Cp^*RhCl_2]_2$ (0.077 g, 0.13 mmol) in *ca.* 15 mL of CH_2Cl_2 containing 30 drops of MeCN was added $AgPF_6$ (0.063 g, 0.25 mmol). After 15 minutes the solution was filtered to remove the AgCl precipitate, and mcbpy (0.050 g, 0.26 mmol) was added to the filtrate. The solution was allowed to stir for 2 hours, the volume was reduced to *ca.* 5 mL, and Et_2O (*ca.* 15 mL) was added, leading to precipitation of an orange solid which was collected by vacuum filtration and found to be the desired complex. Yield: 0.135 g, 85%. ^{1}H NMR (400 MHz, CD_3CN) δ 8.89 (d, $^3J_{H,H}$ = 5.5 Hz, 1H), 8.77 (d, $^3J_{H,H}$ = 6.0 Hz, 1H), 8.47 (d, $^3J_{H,H}$ = 2.2 Hz, 1H), 8.38 (d, $^3J_{H,H}$ = 8.1 Hz, 1H), 8.24 (td, $^3J_{H,H}$ = 7.9 Hz, $^4J_{H,H}$ = 1.5 Hz, 1H), 7.84 (dq, $^3J_{H,H}$ = 6.2 Hz, $^4J_{H,H}$ = 2.9 Hz, 2H), 1.66 (s, 15H) ppm. $^{13}C\{^1H\}$ NMR (126 MHz, CD_3CN) δ 156.39, 154.22, 153.38, 153.08, 149.10, 141.37, 129.82, 129.29, 125.18, 125.08, 98.40 (d, $^1J_{C,Rh}$ = 8.2 Hz, Cp*), 9.13 ppm. ^{19}F NMR (376 MHz, CD_3CN) δ −72.9 (d, $^1J_{F,P}$ = 706 Hz) ppm. ^{31}P NMR (162 MHz, CD_3CN) δ −144.6 ($^1J_{P,F}$ = 706 Hz) ppm. High resolution ESI-MS (positive) *m*/*z*: expected: 463.0215; found: 463.0198 (**1** − $PF6^-$). Anal. calcd for $RhC_{20}H_{22}N_2Cl_2PF_6$: C, 39.43; H, 3.64; N, 4.60. Found: C, 39.44; H, 3.81; N, 4.81. Single crystals of **1** suitable for X-ray diffraction analysis were prepared by vapor diffusion of Et_2O into a solution of the complex in acetonitrile at 5 °C.

Synthesis of [Cp*Rh(mnbpy)Cl]PF_6. To a suspension of $[Cp^*RhCl_2]_2$ (0.073 g, 0.12 mmol) in *ca.* 15 mL of CH_2Cl_2 containing 30 drops of MeCN was added $AgPF_6$ (0.060 g, 0.24 mmol). After 15 minutes the solution was filtered to remove the AgCl precipitate, and mnbpy (0.050 g, 0.25 mmol) was added to the filtrate. The solution was allowed to stir for 2 hours, the volume was reduced to *ca.* 5 mL, and diethyl ether (*ca.* 15 mL) was added, leading to precipitation of a yellow solid which was collected by vacuum filtration and found to be the desired complex. Yield: 0.130 g, 88% yield. ^{1}H NMR (400 MHz, CD_3CN) δ 9.15 (d, $^3J_{H,H}$ = 6.1 Hz, 1H), 9.02 (d, $^3J_{H,H}$ = 2.4 Hz, 1H), 8.92 (d, $^3J_{H,H}$ = 5.5 Hz, 1H), 8.60 (d, $^3J_{H,H}$ = 8.1 Hz, 1H), 8.41 (dd, $^3J_{H,H}$ = 6.1 Hz, $^4J_{H,H}$ = 2.4 Hz, 1H), 8.30 (td, $^3J_{H,H}$ = 7.9 Hz, $^4J_{H,H}$ = 1.5 Hz, 1H), 7.89 (ddd, $^3J_{H,H}$ = 7.5 Hz, $^3J_{H,H}$ = 5.6 Hz, $^4J_{H,H}$ = 1.3 Hz, 1H), 1.68 (s, 15H) ppm. $^{13}C\{^1H\}$ NMR (126 MHz, CD_3CN) δ 155.16, 153.18, 141.54, 130.36, 125.94, 121.86, 98.95 (d, $^1J_{C,Rh}$ = 9.2 Hz, Cp*), 9.15 ppm. ^{19}F NMR (376 MHz, CD_3CN) δ −72.9 (d, $^1J_{F,P}$ = 706 Hz) ppm. ^{31}P NMR (162 MHz, CD_3CN) δ −144.7 ($^1J_{P,F}$ = 706 Hz) ppm. High Resolution ESI-MS (positive) *m*/*z*: expected: 474.0456; found: 474.0473 (**2** − $PF6^-$). Anal. calcd for $RhC_{20}H_{22}N_3O_2ClPF_6$ + H_2O: C, 37.67; H, 3.79; N, 6.59. Found: C, 38.05; H, 3.79; N, 6.57. In order to characterize the molecular cation of **2** by single-crystal XRD analysis, it was crystallized as the triflate salt; diffusion of pentane into an acetone solution of [Cp*Rh(mnbpy)Cl]OTf at −20 °C yielded single crystals suitable for XRD analysis.

Data availability

Data supporting this article have been included as part of the ESI.† Crystallographic data for complexes **1** and **2** have been deposited with Cambridge Crystallographic Data Centre under three accession numbers: 2203159 (**1**, q01i), 2203160 (**2**, a11a-No60) and 2370048 (**2**, a11a-No33), respectively.

Conflicts of interest

There are no conflicts to declare.

Acknowledgements

The authors thank Justin Douglas and Sarah Neuenswander for assistance with NMR spectroscopy, and Chris Malliakas for helpful discussions regarding structure q01i. This work was supported by the US National Science Foundation through award OIA-1833087. J.P.S. was supported by the Beckman Scholars Program at the University of Kansas, funded by the Arnold & Mabel Beckman Foundation. The authors also acknowledge the National Science Foundation for support of the X-ray diffractometer used for collection of the data set for structure q01i (CHE-0923449).

References

1 W. N. G. Moore, W. C. Henke, D. Lionetti, V. W. Day and J. D. Blakemore, *Molecules*, 2018, **23**, 2857.
2 W. Kaim, *Coord. Chem. Rev.*, 1987, **76**, 187–235.
3 V. Lyaskovskyy and B. de Bruin, *ACS Catal.*, 2012, **2**, 270–279.
4 D. Lionetti, V. W. Day, B. Lassalle-Kaiser and J. D. Blakemore, *Chem. Commun.*, 2018, **54**, 1694–1697.

5 S. J. Kraft, P. E. Fanwick and S. C. Bart, *Inorg. Chem.*, 2010, **49**, 1103–1110.
6 J. F. Hull, Y. Himeda, W.-H. Wang, B. Hashiguchi, R. Periana, D. J. Szalda, J. T. Muckerman and E. Fujita, *Nat. Chem.*, 2012, **4**, 383–388.
7 L. Duan, F. Bozoglian, S. Mandal, B. Stewart, T. Privalov, A. Llobet and L. Sun, *Nat. Chem.*, 2012, **4**, 418–423.
8 R. Matheu, M. Z. Ertem, J. Benet-Buchholz, E. Coronado, V. S. Batista, X. Sala and A. Llobet, *J. Am. Chem. Soc.*, 2015, **137**, 10786–10795.
9 D. W. Shaffer, Y. Xie, D. J. Szalda and J. J. Concepcion, *J. Am. Chem. Soc.*, 2017, **139**, 15347–15355.
10 E. Y. Tsui and T. Agapie, *Proc. Natl. Acad. Sci. U.S.A.*, 2013, **110**, 10084–10088.
11 N. P. Mankad, *Chem. Commun.*, 2018, **54**, 1291–1302.
12 P. Sharma, D. R. Pahls, B. L. Ramirez, C. C. Lu and L. Gagliardi, *Inorg. Chem.*, 2019, **58**, 10139–10147.
13 B. G. Cooper, J. W. Napoline and C. M. Thomas, *Catal. Rev.: Sci. Eng.*, 2012, **54**, 1–40.
14 A. Kumar, D. Lionetti, V. W. Day and J. D. Blakemore, *J. Am. Chem. Soc.*, 2020, **142**, 3032–3041.
15 M. R. Norris, J. J. Concepcion, Z. Fang, J. L. Templeton and T. J. Meyer, *Angew. Chem., Int. Ed.*, 2013, **52**, 13580–13583.
16 H. Jaegfeldt, T. Kuwana and G. Johansson, *J. Am. Chem. Soc.*, 1983, **105**, 1805–1814.
17 D. Lionetti, V. W. Day and J. D. Blakemore, *Dalton Trans.*, 2017, **46**, 11779–11789.
18 M. D. Sampson and C. P. Kubiak, *J. Am. Chem. Soc.*, 2016, **138**, 1386–1393.
19 W. C. Henke, D. Lionetti, W. N. G. Moore, J. A. Hopkins, V. W. Day and J. D. Blakemore, *ChemSusChem*, 2017, **10**, 4589–4598.
20 K. A. Grice, J. K. Nganga, M. D. Naing and A. M. Angeles-Boza, in *Comprehensive Coordination Chemistry III*, ed. E. C. Constable, G. Parkin and L. Que Jr, Elsevier, Oxford, 2021, pp. 60–77.
21 W. C. Henke, C. J. Otolski, W. N. G. Moore, C. G. Elles and J. D. Blakemore, *Inorg. Chem.*, 2020, **59**, 2178–2187.
22 W. C. Henke, J. P. Stiel, V. W. Day and J. D. Blakemore, *Chem. – Eur. J.*, 2022, **28**, e202103970.
23 W. C. Henke, J. A. Hopkins, M. L. Anderson, J. P. Stiel, V. W. Day and J. D. Blakemore, *Molecules*, 2020, **25**, 3189.
24 J. Druey and P. Schmidt, *Helv. Chim. Acta*, 1950, **33**, 1080–1087.
25 H. Ohrui, A. Senoo and T. Kosuge, *Preparation of diazafluorene compounds via palladium catalyzed condensation reaction of diazafluorene dihalides with boronic acid derivatives*, US20080161574A1, Canon Kabushiki Kaisha, Japan, 2008, pp. 22.
26 E. A. Boyd, D. Lionetti, W. C. Henke, V. W. Day and J. D. Blakemore, *Inorg. Chem.*, 2019, **58**, 3606–3615.
27 C. G. Comadoll, W. C. Henke, J. A. Hopkins Leseberg, J. T. Douglas, A. G. Oliver, V. W. Day and J. D. Blakemore, *Organometallics*, 2021, **40**, 3808–3818.
28 E. A. Boyd, J. A. Hopkins Leseberg, E. L. Cosner, D. Lionetti, W. C. Henke, V. W. Day and J. D. Blakemore, *Chem. – Eur. J.*, 2022, **28**, e202104389.
29 V. Ganesan, J. J. Kim, J. Shin, K. Park and S. Yoon, *Inorg. Chem.*, 2022, **61**, 5683–5690.
30 U. Kölle and M. Grätzel, *Angew. Chem.*, 1987, **99**, 572–574.
31 U. Kölle, B. S. Kang, P. Infelta, P. Comte and M. Grätzel, *Chem. Ber.*, 1989, **122**, 1869–1880.
32 C. L. Pitman, O. N. L. Finster and A. J. M. Miller, *Chem. Commun.*, 2016, **52**, 9105–9108.
33 L. M. A. Quintana, S. I. Johnson, S. L. Corona, W. Villatoro, W. A. Goddard, M. K. Takase, D. G. VanderVelde, J. R. Winkler, H. B. Gray and J. D. Blakemore, *Proc. Natl. Acad. Sci. U.S.A.*, 2016, **113**, 6409–6414.
34 W. C. Henke, Y. Peng, A. A. Meier, E. Fujita, D. C. Grills, D. E. Polyansky and J. D. Blakemore, *Proc. Natl. Acad. Sci. U.S.A*, 2023, **120**, e2217189120.
35 T. Balduf, J. D. Blakemore and M. Caricato, *J. Phys. Chem. A*, 2023, **127**, 6020–6031.
36 R. Ruppert, S. Herrmann and E. Steckhan, *Tetrahedron Lett.*, 1987, **28**, 6583–6586.
37 R. Ruppert, S. Herrmann and E. Steckhan, *J. Chem. Soc., Chem. Commun.*, 1988, 1150–1151.
38 E. Steckhan, S. Herrmann, R. Ruppert, E. Dietz, M. Frede and E. Spika, *Organometallics*, 1991, **10**, 1568–1577.
39 J. P. Stiel, W. Henke, W. Moore, V. W. Day and J. D. Blakemore, Investigating the synthesis and redox chemistry of [Cp*Rh] complexes supported by monosubstituted bipyridyl ligands. In Abstracts of Papers, American Chemical Society National Meeting, Spring 2022, San Diego, California.
40 A. Baron, C. Herrero, A. Quaranta, M.-F. Charlot, W. Leibl, B. Vauzeilles and A. Aukauloo, *Chem. Commun.*, 2011, **47**, 11011–11013.
41 T. Mizuno, M. Takeuchi, I. Hamachi, K. Nakashima and S. Shinkai, *J. Chem. Soc., Perkin Trans. 2*, 1998, 2281–2288.
42 K. R. Schwartz, R. Chitta, J. N. Bohnsack, D. J. Ceckanowicz, P. Miró, C. J. Cramer and K. R. Mann, *Inorg. Chem.*, 2012, **51**, 5082–5094.
43 C. White, A. Yates and P. M. Maitlis, *Inorg. Synth.*, 1992, **29**, 228–234.
44 M. A. Mantell, J. W. Kampf and M. Sanford, *Organometallics*, 2018, **37**, 3240–3242.
45 C. White, S. J. Thompson and P. M. Maitlis, *J. Chem. Soc., Dalton Trans.*, 1977, 1654–1661.
46 A. Nutton, P. M. Bailey and P. M. Maitlis, *J. Chem. Soc., Dalton Trans.*, 1981, 1997–2002.
47 M. A. Scharwitz, I. Ott, Y. Geldmacher, R. Gust and W. S. Sheldrick, *J. Organomet. Chem.*, 2008, **693**, 2299–2309.
48 W. N. G. Moore, V. W. Day and J. D. Blakemore, CCDC 2202476: Experimental Crystal Structure Determination, 2022, DOI: **10.5517/ccdc.csd.cc2cxvms**.
49 Our preparation of **A** utilized 4-amino-2,2′-bipyridyl prepared according to the procedeure described in the following report: K. Kodama, A. Kobayashi and T. Hirose, *Tetrahedron Lett.*, 2013, **54**, 5514–5517.

50 C. R. Groom, I. J. Bruno, M. P. Lightfoot and S. C. Ward, *Acta Crystallogr., Sect. B: Struct. Sci., Cryst. Eng. Mater.*, 2016, **72**, 171–179.
51 (*a*) K. Heintz, W. Imhof and H. Görls, CCDC 1446087: Experimental Crystal Structure Determination, 2017, DOI: **10.5517/ccdc.csd.cc1kjrzt**; (*b*) C. Schink, A. Catena, K. Heintz, H. Görls, C. Beresko, G. Ankerhold, M. von der Au, B. Meermann, S. J. M. Van Malderen, F. Vanhaecke, S. Wehner, W. Imhof and C. B. Fischer, CCDC 1823616: Experimental Crystal Structure Determination, 2020, DOI: **10.5517/ccdc.csd.cc1z6mb4**.
52 (*a*) Y.-S. Jiao, C.-Q. Jiao, Y.-S. Meng, X.-R. Liu, L. Zhao and T. Liu, CCDC 1816309: Experimental Crystal Structure Determination, 2018, DOI: **10.5517/ccdc.csd.cc1yz0mk**; (*b*) Y.-S. Jiao, C.-Q. Jiao, Y.-S. Meng, X.-R. Liu, L. Zhao and T. Liu, CCDC 1816310: Experimental Crystal Structure Determination, 2018, DOI: **10.5517/ccdc.csd.cc1yz0nl**.
53 P. R. Murray, S. Crawford, A. Dawson, A. Delf, C. Findlay, L. Jack, E. J. L. McInnes, S. Al-Musharafi, G. S. Nichol, I. Oswald and L. J. Yellowlees, *Dalton Trans.*, 2012, **41**, 201–207.
54 W. Kaim, R. Reinhardt, E. Waldhör and J. Fiedler, *J. Organomet. Chem.*, 1996, **524**, 195–202.
55 M. Ladwig and W. Kaim, *J. Organomet. Chem.*, 1992, **439**, 79–90.
56 W. Kaim, R. Reinhardt, E. Waldhoer and J. Fiedler, *J. Organomet. Chem.*, 1996, **524**, 195–202.
57 J. D. Blakemore, E. S. Hernandez, W. Sattler, B. M. Hunter, L. M. Henling, B. S. Brunschwig and H. B. Gray, *Polyhedron*, 2014, **84**, 14–18.
58 P. R. Sharp, D. W. Hoard and C. L. Barnes, *J. Am. Chem. Soc.*, 1990, **112**, 2024–2026.
59 D. W. Hoard and P. R. Sharp, *Inorg. Chem.*, 1993, **32**, 612–620.
60 D. Lionetti, V. W. Day and J. D. Blakemore, *Dalton Trans.*, 2019, **48**, 12396–12406.
61 N. G. Connelly and W. E. Geiger, *Chem. Rev.*, 1996, **96**, 877–910.
62 C. Creutz, *Comments Inorg. Chem.*, 1982, **1**, 293–311.
63 R. K. Harris, E. D. Becker, S. M. Cabral de Menezes, R. Goodfellow and P. Granger, *Pure Appl. Chem.*, 2001, **73**, 1795–1818.
64 R. K. Harris, E. D. Becker, S. M. Cabral De Menezes, P. Granger, R. E. Hoffman and K. W. Zilm, *Pure Appl. Chem.*, 2008, **80**, 59–84.
65 *APEX2, Version 2 User Manual, M86-E01078*, Bruker Analytical X-ray Systems, Madison, WI, June 2006.
66 *SAINT Ver. 8.40A*. Bruker Analytical X-ray Systems Inc., Madison, WI, USA, 2022.
67 G. M. Sheldrick. *SADABS (version 2008/1): Program for Absorption Correction for Data from Area Detector Frames*, University of Göttingen, 2008.
68 L. Krause, R. Herbst-Irmer, G. M. Sheldrick and D. Stalke, *J. Appl. Crystallogr.*, 2015, **48**, 3–10.
69 G. M. Sheldrick, *Acta Crystallogr., Sect. A: Found. Adv.*, 2015, **71**, 3–8.
70 G. Sheldrick, *Acta Crystallogr., Sect. C: Struct. Chem.*, 2015, **71**, 3–8.
71 G. M. Sheldrick, *Acta Crystallogr., Sect. A: Found. Crystallogr.*, 2008, **64**, 112–122.
72 O. V. Dolomanov, L. J. Bourhis, R. J. Gildea, J. A. K. Howard and H. Puschmann, *J. Appl. Crystallogr.*, 2009, **42**, 339–341.
73 C. B. Hübschle, G. M. Sheldrick and B. Dittrich, *J. Appl. Crystallogr.*, 2011, **44**, 1281–1284.